peptide SEGYTFQVQDGAPGTFNF coupled to keyhole limpet hemocyanin and against full-length recombinant hSRP1α expressed in *E. coli* (Fig. 3A). Standard immunization procedures were used.
33. Immunopurification was performed by recycling 10 ml of HeLa S100 extract (~10 mg/ml), prepared according to the method described by Dignam *et al.* [J. D. Dignam, R. M. Lebovitz, R. G. Roeder, *Nucleic Acids. Res.* **11**, 1475 (1983)], over a 1-ml column of protein A–Sepharose 4B beads (Pharmacia) coupled to either preimmune or antipeptide antiserum, for 2 hours at 4°C. The beads were washed with 50 ml of IPP buffer and then eluted by incubation of the beads for 2 hours at room temperature in 1 ml of IPP buffer containing free hSRP1α peptide (1 mg/ml).
34. For MonoQ chromatography, eluates of the affinity column were dialyzed for 2 hours at 4°C against 500 ml of IPP buffer without Triton X-100 and peptide. The dialyzate was loaded directly onto a MonoQ PC1.6/5 column through use of the SMART system (Pharmacia) and eluted with a gradient from 150 to 600 mM NaCl in 20 column volumes. The hSRP1α complex eluted in a sharp peak at ~300 mM NaCl.
35. The hSRP1α expression vector was constructed by subcloning of a Bam HI–Xho I fragment of a Bluescript plasmid vector containing the full-length hSRP1α cDNA (pBShSRP1α) inserted between the Bam HI and Xho I sites of the His vector pRSET (Invitrogen). The resulting plasmid, pHish-SRP1α, was grown in *E. coli* strain BL21LysS to an absorbance at 600 nm ($A_{600}$) of 0.4 and induced with isopropyl-β-D-thiogalactopyranoside for 3 hours at 30°C. Cells from a 3-liter culture were lyzed with a French Press and recombinant hSRP1α purified twice over Ni–nitrilotriacetic acid agarose (Qiagen) under native conditions.
36. Immunoprecipitations were done as described (*29*). $^{35}$S-labeled CBP80 and CBP80-NLS2 were prepared by in vitro translation with rabbit reticulocyte lysate (Promega).
37. Import assays were done essentially as described by Adam *et al.* (*4*) except that HeLa cells were permeabilized in suspension with digitonin. All samples were incubated at 23°C for 60 min in a total volume of 10 μl in a buffer containing 20 mM Hepes-KOH (pH 7.3), 110 mM potassium acetate, 5 mM sodium acetate, 2 mM magnesium acetate, 1 mM EGTA, 2 mM dithiothreitol, 1 mM phenylmethylsulfonyl fluoride (all final concentrations) with ~$10^4$ cells per assay. The samples indicated contained ATP and GTP (guanosine triphosphate) (each at 2 mM), creatine phosphate (10 mM), and creatine kinase (1 μg/ml) (all final concentrations). Hexokinase was used at 20 U/ml final concentration. *Xenopus* egg extracts were prepared essentially as described [M. J. Lohka and Y. Masui, *Science* **220**, 719 (1984)].
38. We are grateful to C. Dingwall, E. Izaurralde, I. Palacios, and C. McGuigan for discussions and help with the in vitro transport assays and for sharing reagents. We are also grateful to R. Brent and T. Kreis for providing HeLa cDNA libraries, to J. Lewis for help with fractionation procedures, and to M. Nomura for providing yeast strains. We thank C. Calvio, S. Kandels-Lewis, G. Lamm, N. Santama, B. Seraphin, and our other colleagues for helpful discussions and for critical comments on the manuscript. K.W. was supported by a predoctoral stipend from Boehringer Ingelheim Fonds.

26 January 1995; accepted 6 March 1995

# Photovoltage of Rods and Cones in the Macaque Retina

David M. Schneeweis and Julie L. Schnapf*

**The kinetics, gain, and reliability of light responses of rod and cone photoreceptors are important determinants of overall visual sensitivity. In voltage recordings from photoreceptors in an intact primate retina, rods were found to be functionally isolated from each other, unlike the tightly coupled rods of cold-blooded vertebrates. Cones were observed to receive excitatory input from rods, which indicates that the cone pathway also processes rod signals. This input might be expected to degrade the spatial resolution of mesopic vision.**

The photocurrent signals of photoreceptor cells primarily reflect light-activated biochemical processes that occur in the outer segment. The membrane potential, however, also can be shaped by voltage-dependent conductances and synaptic interactions (*1*). This study demonstrates a role for these latter processes in primate photoreceptors. These processes are of particular importance because the photovoltage, not the photocurrent, modulates synaptic transmission.

Photovoltage responses of 16 rods and 23 cones (14 green and 9 red) from 13 monkeys were measured with the perforated-patch technique (*2*). Dark-adapted retinas, obtained primarily from the monkey *Macaca fascicularis*, were placed in a recording chamber and superfused with physiological saline (*3*). A 180- or 400-μm-diameter spot of plane-polarized light, incident on the ganglion cell side of the retina, was focused onto the photoreceptors. The rate of photoisomerization was estimated from the product of the light intensity and the collecting area, $A_c$, of the photoreceptor (*4*).

The dark resting potential of rods was, on average, −37 mV, and light evoked hyperpolarizing responses that increased with flash strength (Fig. 1, A and B). The relation between peak hyperpolarization and photon density was fitted by a Michaelis function (Fig. 1C). This function is less steep than the exponential saturation function that describes the intensity dependence of the photocurrent in macaque and human rods (*5*, *6*). The photon density that elicited a response of half-maximal amplitude was 75 ± 40 photons μm$^{-2}$ (mean ± SD, $n$ = 10), or about 75 photoisomerizations. Input resistance was 1.2 ± 0.5 gigohms (mean ± SD, $n$ = 6) (*7*).

The time to the peak of the response to the flash decreased with increasing flash strength from 200 ms to less than 35 ms (Fig. 1, A and B). In response to bright flashes, the photovoltage displayed an initial transient that decayed to a plateau of intermediate value. These kinetic features are not present in the photocurrent (*5*); differences of this kind between photocurrent and voltage have been observed previ-

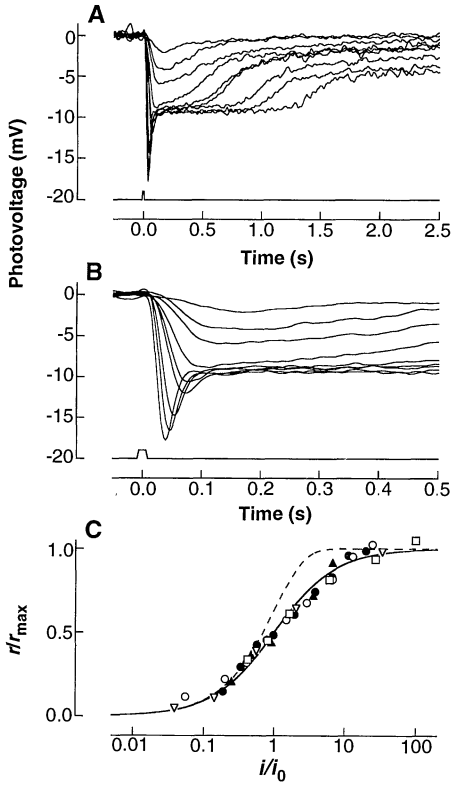


**Fig. 1.** Dependence of photovoltage on flash strength in macaque rods. Change in membrane potential in one rod is plotted in (**A**) and (**B**), on two time scales, as a function of time after the middle of a 10-ms flash. Traces are average responses to 1 to 18 flashes. Dark resting membrane potential is −43 mV. Response bandwidth, DC to 30 Hz. Flash monitor is below voltage traces. Flash photon densities ranged from 5 photons μm$^{-2}$ to 2300 photons μm$^{-2}$, at 500 nm. (**C**) Peak hyperpolarization of five rods is plotted as a function of flash strength on normalized axes. Each symbol represents a different cell; $r$, peak hyperpolarization; $r_{max}$, maximal hyperpolarization to a saturating light; $i$, flash photon density; $i_0$, the photon density that elicited a peak response of ½$r_{max}$. For the cells plotted, $r_{max}$ varied between 13 mV and 35 mV (mean 22 mV) and $i_0$ ranged from 17 photons μm$^{-2}$ to 130 photons μm$^{-2}$. The continuous curve is the Michaelis function, $r/r_{max} = i/(i + i_0)$; the dashed curve is an exponential saturation function, $r/r_{max} = 1 - \exp(-i/i_0)$.

Departments of Ophthalmology and Physiology, University of California, San Francisco, CA 94143–0730, USA.

*To whom correspondence should be addressed.

ously in the rods of amphibians and were attributed to voltage-dependent conductances (*1*).

In cold-blooded vertebrates, rods are coupled to each other extensively through electrical synapses (*8, 9*). This mechanism effectively averages the signals of many rods, thereby reducing variability in the amplitude of responses to dim flashes (*8*). In this study, however, we found that the amplitude variability in monkey rods was comparatively large (Fig. 2A), which suggests that neighboring rods are not tightly coupled. The number of effectively coupled rods, $N_e$, defined as the ratio of the expected variance of an isolated rod to the measured ensemble variance, was estimated from responses to dim flashes (*9–11*). For the rod in Fig. 2, $N_e$ was 1.2. In a total of five rods, $N_e = 0.6 \pm 0.4$ (mean ± SD), close to the value of 1, which denotes an absence of coupling. In contrast, for the rod network of cold-blooded vertebrates (*8, 9*), $N_e \cong 10$ to 30. The absence of rod coupling observed here in primate retina is consistent with the absence of gap junctions between primate rods (*12*).

If the rods are electrically isolated and each photoisomerization elicits an identical voltage response, it is expected that the waveform of the ensemble variance would match that of the square of the average response (*13*). For monkey rods, this expectation was met for times up to and slightly past the time to peak, but deviations were observed at later times, when the variance was consistently larger than predicted (Fig. 2C). A corresponding variation in the duration of the flash responses can be seen directly (Fig. 2A). A similar dispersion in time course has been observed in photocurrent responses of monkey rods [figure 6 in (*5*)], which suggests that variability may exist in the biochemical processes that turn off the photon response. Some variability in the time course might be expected from variations in the longitudinal position of photon absorption within the outer segment (*5, 13*). The mechanism responsible for this positional dependence is not known.

Assuming that rods are electrically independent, several estimates of the mean peak hyperpolarization per photoisomerization, *a*, were derived from responses to dim flashes. One estimate was obtained from the ratio of the peak ensemble variance $\sigma^2$ (Fig. 2C) to the peak amplitude of the mean $\mu$ (Fig. 2B). For the rod in Fig. 2, this gave a value for *a* of 1.1 mV. A second estimate was obtained from the distribution of response amplitudes (Fig. 2D, bars). This function was well described by a Poisson distribution of photoisomerizations (Fig. 2D, curve) that was smoothed by dispersion in the size of the single photon response and by baseline noise (*14, 15*). The value of *a* that gave the best fit of the theoretical distribution to the measured histogram was 1.5 mV for the rod in Fig. 2, and 1.2 ± 0.3 mV (mean ± SD) in a total of five rods. This is close to the value of 1.1 ± 0.4 mV obtained from the variance to mean ratio in the same collection of rods. It also is similar to the value of 0.7 ± 0.4 mV obtained from $a = \mu/(iA_c)$, where $A_c$ was taken as 1 $\mu m^2$ and *i* is the flash photon density. The reasonable agreement of the three estimates supports the theory that variations in the photovoltage reflected variations in the number of photoisomerizations of a single rod and that the peak response amplitude per photoisomerization was about 1 mV. This magnitude is similar to that of rods in cold-blooded vertebrates (*8, 9*).

The dark resting potential of cones was, on average, −46 mV. The intensity dependence of response amplitude followed a Michaelis function (Fig. 3C). Half-maximal amplitudes were evoked by 1430 ± 870 photoisomerizations (mean ± SD, $n = 9$) (*16*). The single photon response amplitude *a* was estimated to be 5.2 ± 3.7 $\mu$V (mean ± SD, $n = 10$) from extrapolations of the Michaelis function. Maximal hyperpolarizations ranged from 5 to 12 mV; these values were somewhat smaller than those reported for turtle cones (*11, 17*). Lower values

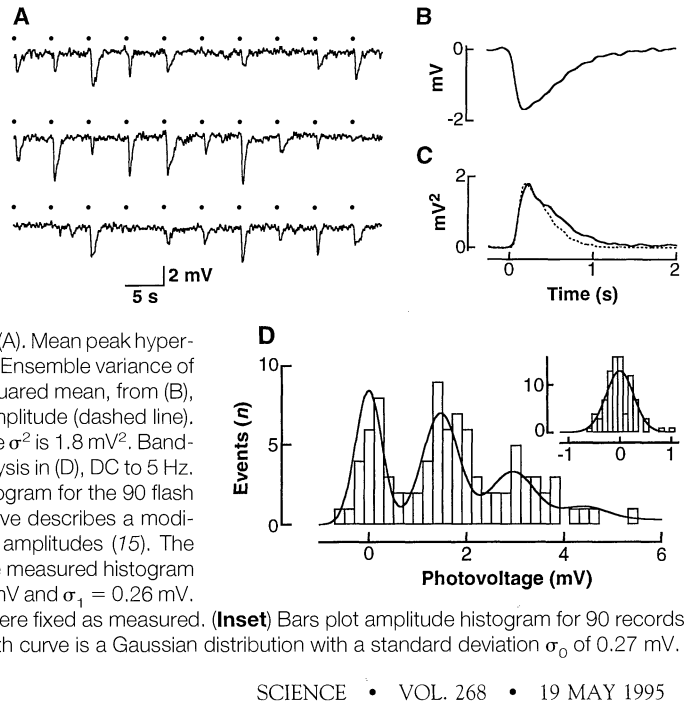


**Fig. 2.** Amplitude fluctuations of a rod in dim light, 10-ms flashes, 500 nm, 1.3 photons $\mu m^{-2}$; $r_{max}$ = 25 mV; resting potential is −37 mV. (**A**) Photovoltage responses to flashes; dots indicate the timing of flashes. Bandwidth, DC to 3 Hz. (**B**) Ensemble average photovoltage for responses to 90 flashes, including those illustrated in (A). Mean peak hyperpolarization $\mu$ is 1.7 mV. (**C**) Ensemble variance of photovoltage (solid line). Squared mean, from (B), scaled to the same peak amplitude (dashed line). The peak change of variance $\sigma^2$ is 1.8 $mV^2$. Bandwidth in (B) and (C) and analysis in (D), DC to 5 Hz. (**D**) Bars plot amplitude histogram for the 90 flash responses. The smooth curve describes a modified Poisson distribution of amplitudes (*15*). The best (least squares) fit to the measured histogram was achieved with $a = 1.5$ mV and $\sigma_1 = 0.26$ mV. The parameters $\mu$ and $\sigma_0$ were fixed as measured. (**Inset**) Bars plot amplitude histogram for 90 records in darkness (*15*). The smooth curve is a Gaussian distribution with a standard deviation $\sigma_0$ of 0.27 mV.

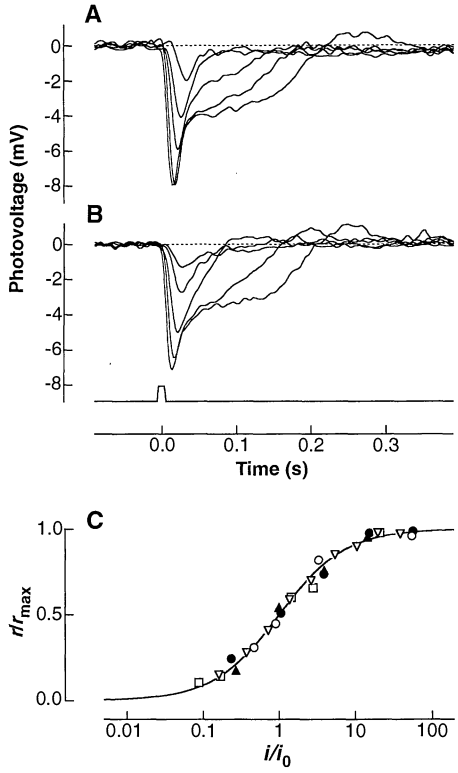


**Fig. 3.** Dependence of photovoltage on flash strength in macaque cones. Change in membrane potential of a red cone is plotted as a function of time after the middle of a 10-ms flash of 500-nm (**A**) or 660-nm (**B**) light. Traces are the average responses to 1 to 12 flashes. Flashes at the two wavelengths were interleaved. Flash monitor is shown below the voltage traces in (B). Flash photon densities ranged from 340 photons $\mu m^{-2}$ to 8.15 × $10^4$ photons $\mu m^{-2}$ in (A) and 8.17 × $10^3$ photons $\mu m^{-2}$ to 8.24 × $10^5$ photons $\mu m^{-2}$ in (B). Resting membrane potential in the dark was −47 mV. Bandwidth, DC to 50 Hz. (**C**) Peak hyperpolarization from two red cones (filled symbols) and three green cones (open symbols) plotted as a function of flash strength on normalized axes. Each symbol denotes a different cell. For the cells shown, $r_{max}$ ranged from 5 mV to 11 mV, and $i_0$ (at 500 nm) ranged from 550 photons $\mu m^{-2}$ to 2140 photons $\mu m^{-2}$ for the green cones, and 1440 photons $\mu m^{-2}$ to 5750 photons $\mu m^{-2}$ for the red cones. The curve is the Michaelis function.

could result from electrical coupling between a cone and its numerous neighboring rods.

In some cells (Fig. 3), the photovoltage displayed a depolarizing overshoot, presumably because of a delayed increase in the light-activated conductance of the outer segment (*18*); a corresponding inward current was observed in voltage clamp. In contrast with the photocurrent, the time to the peak photovoltage (Fig. 3, A and B) varied with intensity, from about 35 ms for dim flashes to less than 10 ms for flashes of saturating intensities. In response to bright flashes, the photovoltage showed an initial spike that decayed to a plateau. These characteristics of the photovoltage, which are absent from the photocurrent (*18*), likely are attributable to the voltage-gated channels previously described in macaque cones (*19*).

Unlike the photocurrent (*20*), the waveform of the cone photovoltage was dependent on wavelength. When intensities of 500- and 660-nm light were adjusted to evoke responses of comparable peak amplitude, the 500-nm response was longer-lasting and displayed a prominent hyperpolarizing after potential (Figs. 3 and 4A). When light intensities were readjusted to equate photon absorption in rods (*21*), the resultant after-potentials were equivalent at the two wavelengths (Fig. 4B). In addition to the rod-like spectral sensitivity, the intensity dependence, duration and adaptation characteristics (*22*) of the after-hyperpolarization are consistent with the idea that rod signals modulate the membrane potential of cones.

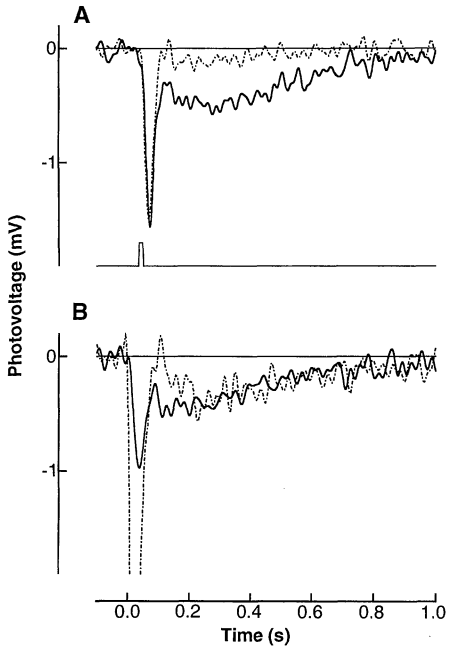


**Fig. 4.** Cone photovoltage has a rod component. Each trace is the average of four to nine responses of a green cone to a 10-ms flash of 500-nm (solid curves) or 660-nm (dashed curves) light. Flashes at the two wavelengths were interleaved. (**A**) Flash strengths were adjusted to evoke responses of comparable peak amplitude: 178 photons $\mu m^{-2}$ (500 nm) and $5.45 \times 10^4$ photons $\mu m^{-2}$ (660 nm). The response at 500 nm had a prominent hyperpolarizing after-potential. (**B**) Flash strengths were adjusted to evoke equal photon absorption for rods: 94 photons $\mu m^{-2}$ (500 nm) and $4.30 \times 10^5$ photons $\mu m^{-2}$ (660 nm). Response to the 660-nm flash was truncated. Bandwidth, DC to 40 Hz. Resting potential is −48 mV; $r_{max}$ = 8.2 mV.

Rods appeared to contribute to the early phase of the cone response as well. In both red ($n$ = 6) and green ($n$ = 8) cones, peak sensitivity at 500 nm relative to 660 nm was on average two times greater than that expected from photocurrent recordings (*20, 21*). In contrast, the relative sensitivity measured in four rods was within 5% of that expected from previous spectral sensitivity measurements (*5, 21*). Evidence for rod input was obtained in all 20 cones tested and probably is mediated by the gap junctions observed between rods and cones in the macaque retina (*12*). The absence of a detectable cone contribution to the rod membrane potential is expected, because the rods outnumber the cones by a factor of 20 in the region of the retina studied. Rod input to cones has been observed previously in a study of a small number of cones in the cat retina (*23*).

It has been hypothesized from human psychophysical experiments that rod signals are transmitted via two distinct retinal pathways (*24*). One pathway dominates at low light levels. The second pathway has faster bandpass temporal properties and dominates at mesopic light levels. The rod input we observed in cones may reflect the entry point for rod signals into this second rod pathway, whereas the direct rod-to-bipolar synapse would constitute the origin of the slower pathway (*23–25*). If that is so, differences between rods and cones in the gain and temporal filter characteristics of the synapses with their second-order cells (*26*) might account for the observed temporal and sensitivity differences of the two psychophysical pathways.

## REFERENCES AND NOTES


1. D. A. Baylor, M. G. F. Fuortes, P. M. O'Bryan, *J. Physiol. (London)* **214**, 265 (1971); C. R. Bader, P. R. MacLeish, E. A. Schwartz, *ibid.* **296**, 1 (1979); C. R. Bader, D. Bertrand, E. A. Schwartz, *ibid.* **331**, 253 (1982); D. A. Baylor and B. J. Nunn, *ibid.* **371**, 115 (1986).
2. R. Horn and A. Marty, *J. Gen. Physiol.* **92**, 145 (1988). Recordings from inner segments of rods and cones were made with electrodes filled with a solution that contained 130 mM potassium gluconate, 10 mM KCl, 4 mM $MgCl_2$, 3 mM adenosine triphosphate · $Na_2$, 1 mM guanosine triphosphate · $Na_3$, 10 mM Hepes buffer (pH = 7.25), and 130 μM amphotericin. Voltage or current was measured with an Axopatch 1C amplifier (Axon Instruments) and filtered by analog filters; resultant phase delays were taken into account. Voltage traces in some figures were filtered by a Gaussian digital filter whose bandwidth was selected to minimize instrumental noise without causing a detectable change in the waveform or amplitude of the signal. Membrane potentials were corrected for the electrode junction potential.
3. Enucleations were performed on animals anesthetized with $N_2O:O_2$ (1:1) and 1 to 3% isoflurane. Dark-adapted retinas were prepared as described previously (*18*). A piece of peripheral retina was placed photoreceptor side up in the recording chamber, incubated for 3 min in hyaluronidase (50 U/ml), and superfused at 37°C with Lockes solution that contained 120 mM NaCl, 20 mM $NaHCO_3$, 3.6 mM KCl, 2.4 mM $MgCl_2$, 1.2 mM $CaCl_2$, 10 mM dextrose, 3.0 mM Hepes buffer (pH = 7.4), and Basal Medium Eagle amino acids and vitamins (Gibco). Two (of thirteen) monkeys used were *Macaca mulatta*. Data from the two species were comparable and have been pooled.
4. The collecting area $A_c$ (at the wavelength of maximum sensitivity) for rods was taken to be 1 $\mu m^2$ (*5*). This value is about one-half of that calculated previously (*6*) for optimal conditions of axial illumination. The reduced value was chosen to take into account the misalignment of rods with the incident angle of illumination, which would lower the absorption of the plane-polarized light, and reduce the degree to which the inner segment focuses light into the outer segment. The collecting area for cones was taken as 0.6 $\mu m^2$, by analogy with the rods, a value somewhat lower than that expected under optimal optical conditions (*18, 20*). Details of wavelength and intensity control of the light stimuli are given elsewhere (*6*).
5. D. A. Baylor, B. J. Nunn, J. L. Schnapf, *J. Physiol. (London)* **387**, 575 (1984).
6. T. W. Kraft, D. M. Schneeweis, J. L. Schnapf, *ibid.* **464**, 747 (1993).
7. Input resistance was estimated as the ratio of peak photovoltage (in current clamp) to peak photocurrent (in voltage clamp) for near-saturating flashes. A second estimate, from responses to dim flashes, was about two times larger.
8. G. L. Fain, *Science* **187**, 838 (1975).
9. P. B. Detwiler, A. L. Hodgkin, P. A. McNaughton, *J. Physiol. (London)* **300**, 213 (1980).
10. $N_e = \sigma_i^2/\sigma^2$, where $\sigma^2$ is the measured peak ensemble variance for a series of responses to dim flashes and $\sigma_i^2$ is the expected variance of an isolated rod. $\sigma_i^2$ is given by $\mu^2/(iA_c)$, where $i$ is the flash photon density, $\mu$ is the mean peak hyperpolarization, and $A_c$ is the collecting area as defined above.
11. T. D. Lamb and E. J. Simon, *ibid.* **263**, 257 (1976).
12. E. Raviola and N. B. Gilula, *Proc. Natl. Acad. Sci. U.S.A.* **70**, 1677 (1973); R. Nelson, T. Lynn, A. Dickerson-Nelson, H. Kolb, in *Neurocircuitry of the Retina, A Cajal Memorial*, A. Gallego and P. Gouras, Eds. (Elsevier, New York, 1985), pp. 109–121.
13. J. L. Schnapf, *J. Physiol. (London)* **343**, 147 (1983).
14. D. A. Baylor, T. D. Lamb, K.-W. Yau, *ibid.* **288**, 613 (1979).
15. Peak response amplitudes were estimated by scaling the amplitude of the ensemble mean (Fig. 2B) to make the best (least squares) fit to each response (*14*). Fitting was done over the time period when the time courses of the variance and mean-squared response matched. Amplitudes were assumed to be distributed according to a modified Poisson distribution (smooth curve of Fig. 2D), with a mean number of photoisomerizations given by $\mu/a$ [equation 10 in (*14*)]. A Poisson distribution was smoothed by two noise sources: $\sigma_0$, which is the standard deviation of the noise in the dark, and $\sigma_1$, which is the standard deviation of the amplitude dispersion of the single-photon response. Variables $a$ and $\sigma_1$ were free parameters chosen to give the best fit between the measured histogram and the curve; $\mu$ was fixed to the value measured from the mean flash response; and $\sigma_0$ was fixed to the value determined separately from measurements of the membrane potential during time intervals between flashes.
16. The values of the photon densities that elicited peak responses of half-maximal amplitude for the two spectral types of cone were 1070 ± 340 photoisomerizations (mean ± SD, $n$ = 5) for green cones and 1870 ± 1180 photoisomerizations ($n$ = 4) for red cones.

17. D. A. Baylor and A. L. Hodgkin, *J. Physiol. (London)* **234**, 163 (1973).
18. J. L. Schnapf, B. J. Nunn, M. Meister, D. A. Baylor, *ibid.* **427**, 681 (1990).
19. T. Yagi and P. R. MacLeish, *J. Neurophysiol.* **71**, 656 (1994).
20. D. A. Baylor, B. J. Nunn, J. L. Schnapf, *J. Physiol. (London)* **390**, 145 (1987).
21. For rods, the sensitivity at 660 nm compared to that at 500 nm was taken as $2.6 \times 10^{-4}$. Relative sensitivity values were calculated from rod suction electrode recordings (5) after correction for axial illumination by applying Beer's law and assuming a peak axial optical density of 0.35 (5). For cones, the sensitivity at 660 nm relative to that at 500 nm was estimated to be 0.13 (red cone) and $7.4 \times 10^{-3}$ (green cone). Values from suction recordings (*20*) were corrected assuming a peak axial density of 0.17.
22. The after-hyperpolarization could be selectively eliminated by background lights expected to desensitize rods but not cones.
23. R. Nelson, *J. Comp. Neurol.* **172**, 109 (1977).
24. J. D. Conner and D. I. A. MacLeod, *Science* **195**, 698 (1977); J. D. Conner, *J. Physiol. (London)* **332**, 139 (1982); R. Knight and S. L. Buck, *Vision Res.* **33**, 2203 (1993).
25. R. G. Smith, M. A. Freed, P. Sterling, *J. Neurosci.* **6**, 3505 (1986).
26. D. A. Baylor and R. Fettiplace, *Cold Spring Harbor Symp. Quant. Biol.* **40**, 529 (1976); J. L. Schnapf and D. R. Copenhagen, *Nature* **296**, 862 (1983); D. R. Copenhagen, J. F. Ashmore, J. L. Schnapf, *Vision Res.* **4**, 363 (1983).
27. We thank D. A. Baylor, S. L. Buck, D. R. Copenhagen, J. C. Horton, J. H. LaVail, and A. Stockman for comments on the manuscript. This work was funded by a grant from the Plum Foundation and grants RO1–EY07642 and F32–EY06399 from the National Eye Institute. Additional support was obtained from That Man May See and Research to Prevent Blindness.

4 October 1994; accepted 23 February 1995

# Ribosomal RNA Precursor Processing by a Eukaryotic U3 Small Nucleolar RNA–Like Molecule in an Archaeon

Simon Potter, Peter Durovic, Patrick P. Dennis*

An RNA-containing endonuclease that catalyzes the excision and maturation of the 16S ribosomal RNA (rRNA) from the rRNA primary transcript (pre-rRNA) in the hyperthermophilic archaeon *Sulfolobus acidocaldarius* has been characterized. The ribonucleoprotein was inactivated by micrococcal nuclease treatment and inactivation was reversed by reconstitution with bulk RNA. A 159-nucleotide RNA with sequence and structural similarity to U3 small nucleolar RNAs of eukaryotes copurified with the endonuclease activity. Oligonucleotide-targeted ribonuclease H inactivation of the U3-like RNA component also abolished processing activity. A motif within the U3 homolog is complementary to the region around the three cleavage sites in the pre-RNA substrate. Thus, U3-mediated processing of pre-rRNA is not specific to eukaryotes; its origin predates the divergence of archaea and eukaryotes.

At least two endonuclease activities participate in the processing of the primary transcript from the single copy 16S-23S rRNA operon in *S. acidocaldarius* (*1*). The first of these endonucleases is the well-characterized, helix-processing enzyme unique to all archaea (*2*, *3*). This endonuclease excises introns from intron-containing tRNA and rRNA gene transcripts and, in most species, excises pre–16S and 23S rRNAs from the primary rRNA transcript (*1*–*4*). The enzyme has a rigorously defined substrate specificity; it acts on two three-base bulges, located on opposite strands within an extended helix, that are separated by 4 base pairs (bp). With respect to rRNA processing, the enzyme is analogous (but not homologous) to the helix-specific ribonuclease (RNase) III of bacteria (*5*). In *S. acidocaldarius*, this activity excises pre–23S but not pre–16S RNA from the primary rRNA transcript (*1*).

Although the 16S RNA sequence is surrounded by a long inverted repeat in the primary transcript, it is unlikely that the putative helix is used or required for excision or maturation events in the 5′ external transcribed spacer (ETS). Instead, the 5′ ETS is cleaved at three positions by the second endonuclease activity, which we now show resembles the U3-containing ribonucleoprotein (RNP) particles responsible for processing of pre-rRNA in the nucleolus of eukaryotic cells (*6*). The first two cleavages occur ~99 and 31 nucleotides (nt) upstream of the 16S RNA sequence, and the third occurs at the 5′ ETS–16S RNA junction in order to produce the 5′ end of mature 16S RNA. We have shown previously that a cell-free extract of *S. acidocaldarius* will cleave a synthetic RNA substrate that contains the 5′ ETS and the first 72 nt of 16S RNA sequence at or close to the expected three positions (*1*). This observation indicates that 5′ ETS processing does not require formation of the 16S RNA processing helix, and that maturation at the 5′ end of 16S RNA requires no more than 72 nt of 16S RNA sequence and does not require concomitant small ribosomal subunit assembly. The endonuclease activity was sensitive to RNase A digestion, indicating that it contained an RNA component essential for activity.

Primer extension analysis was used to position precisely the 5′ ends of intermediates and products resulting from in vitro cleavage of an SP6 RNA polymerase–transcribed substrate RNA by an activity purified from cell-free extract (*7*) (Fig. 1). The primer was complementary to positions 57 to 35 of 16S rRNA. The observed products indicated that major cleavages occur at positions −99 (site 1) and −31 (site 2) of the 5′ ETS and at position +1 (site 4) at the 5′ ETS–16S RNA junction. These intermediates and the mature 16S RNA product were virtually identical to those observed in vivo (*1*, *8*). Additional minor extension products with 5′ ends near sites 1, 2, and 4 were observed; these could represent alternative positions for endonucleolytic processing or, in some instances, nuclease trimming at the 5′ end of the intermediates or products.

We also directly visualized the accumulation of product fragments that resulted from the cleavage of $^{32}$P-labeled substrate RNA. Three of the four products accumulated in a time-dependent manner (Fig. 2, A and B). The fourth product was too short to visualize on the electrophoresis gel.

RNase A sensitivity of processing activity in crude cell extracts (*1*) was supported by incubating partially purified processing activity with micrococcal nuclease at 37°C before increasing the temperature to 75°C for 15 min and then adding the substrate RNA (*9*). No specific processing was evident when the partially purified activity was treated with the nuclease (Fig. 2C, lanes 2 and 3). The inactivated processing activity was then reactivated by reconstitution with bulk *S. acidocaldarius* RNA (3 to 15 μg) for 15 min at 75°C, after which substrate RNA was added and incubation was continued for a further 15 min at 75°C (Fig. 2C, lanes 4 to 8). Reactivation was partial with the use of 6 μg of RNA and essentially complete with >6 μg of RNA. Bulk RNA from several other archaeal or bacterial species was ineffective in heterologous reconstitution (*7*). The reconstituted activity was itself sensitive to redigestion by micrococcal nuclease. The reconstituted mixture was transferred back to 37°C and a second dose of micrococcal nuclease (100 ng or 1 μg) was added, before returning the sample again to 75°C and adding substrate RNA; no processing was evident (Fig. 2C, lanes 9 to 12).

The presence of an RNA component in the purified processing activity was detected

Department of Biochemistry and Molecular Biology and Canadian Institute for Advanced Research, University of British Columbia, Vancouver, British Columbia, Canada V6T 1Z3.

*To whom correspondence should be addressed.